

Breaking Memory Limits: Gradient Wavelet Transform Enhances LLMs Training

Ziqing Wen¹, Ping Luo¹, Jiahuan Wang¹, Xiaoge Deng¹,
Jinping Zou¹, Kun Yuan², Tao Sun^{1*†}, Dongsheng Li^{1*†}

¹College of Computer Science and Technology, National University of Defense Technology, Changsha, Hunan, China.

²Center for Machine Learning Research, Peking University, Beijing, China.

*Corresponding author(s). E-mail(s): suntao.saltfish@outlook.com;
dqli@nudt.edu.cn;

Contributing authors: zqwen@nudt.edu.cn; luoping@nudt.edu.cn;
wangjiahuan@nudt.edu.cn; dengxg@nudt.edu.cn;
zoujinpjng@nudt.edu.cn; kunyuan@pku.edu.cn;

†These authors contributed equally to this work.

Abstract

Large language models (LLMs) have shown impressive performance across a range of natural language processing tasks. However, their vast number of parameters introduces significant memory challenges during training, particularly when using memory-intensive optimizers like Adam. Existing memory-efficient algorithms often rely on techniques such as singular value decomposition projection or weight freezing. While these approaches help alleviate memory constraints, they generally produce suboptimal results compared to full-rank updates. In this paper, we investigate the memory-efficient method beyond low-rank training, proposing a novel solution called Gradient Wavelet Transform (GWT), which applies wavelet transforms to gradients in order to significantly reduce the memory requirements for maintaining optimizer states. We demonstrate that GWT can be seamlessly integrated with memory-intensive optimizers, enabling efficient training without sacrificing performance. Through extensive experiments on both pre-training and fine-tuning tasks, we show that GWT achieves state-of-the-art performance compared with advanced memory-efficient optimizers and full-rank approaches in terms of both memory usage and training performance.

Keywords: Large language models, memory-efficient training, wavelet transform.

1 Introduction

Large Language Models (LLMs) have made remarkable strides since the release of ChatGPT, a groundbreaking chatbot based on LLM technology [1]. Their promising performance and scalability have led to rapid adoption across a range of interdisciplinary fields, including science [2–4], medicine [5–8], and policy-making in biology [9]. The impressive capabilities of LLMs arise from their vast number of parameters and the massive datasets used for training. However, training these models imposes significant demands on the optimizer, with Adam [10] emerging as the most commonly used optimizer due to its fast convergence, robustness, and strong experimental results.

Despite these advantages, Adam’s memory requirements present a major drawback. Specifically, it consumes twice the memory of the model itself (as illustrated in Figure 1), making memory usage a key bottleneck in LLM training. For instance, pre-training a LLaMA 7B [11] model requires approximately 58GB of GPU memory: 14GB for model weights, 14GB for gradients, 2GB for activations, and 28GB for Adam optimizer states under BF16 precision [12]. When the model size exceeds 100B parameters, as with GPT-3 [1] (175B parameters), the additional memory overhead from Adam can exceed 350GB, requiring at least five additional NVIDIA A100 80GB GPUs.

Given the high costs of training LLMs, methods that reduce the batch size or use larger GPUs quickly become unsustainable. To mitigate these issues, many studies have focused on optimizing memory usage during large-scale model training. A promising solution is low-rank training [12, 13], which has made significant progress in alleviating memory constraints. These memory-efficient methods can be broadly classified into two categories: weight-based and gradient-based approaches [14]. Notable examples include Low-Rank Adaptation (LoRA) [13] and Gradient Low-Rank Projection (GaLore) [12].

LoRA leverages the low-rank nature of model parameter updates by freezing the pre-trained model weights and reparameterizing weight updates with trainable low-rank decomposition matrices. Extensive experiments have demonstrated that LoRA is effective in fine-tuning tasks, but its performance in pre-training remains limited. Additionally, the strong low-rank assumptions underlying LoRA often lead to suboptimal outcomes [15, 16]. To address these limitations, Re-LoRA [17] extends LoRA’s applicability to pre-training by periodically updating the frozen model parameters. However, this periodic update process requires full-rank training, which significantly undermines the memory efficiency gains Re-LoRA could otherwise achieve [12].

In contrast to LoRA, which decomposes the update matrix, GaLore reduces the optimizer state memory usage by performing Singular Value Decomposition (SVD) on the gradients, since the memory occupied by optimizer states is directly tied to the gradient size (as shown in Figure 1). GaLore has demonstrated effective performance in both pre-training and fine-tuning tasks. However, its performance still lags behind that of full-rank methods, and it only captures information within the projected subspace, discarding gradient information outside of it. This limitation becomes particularly problematic when using lower ranks or when gradients are noisy, leading to significant convergence issues [12, 18].

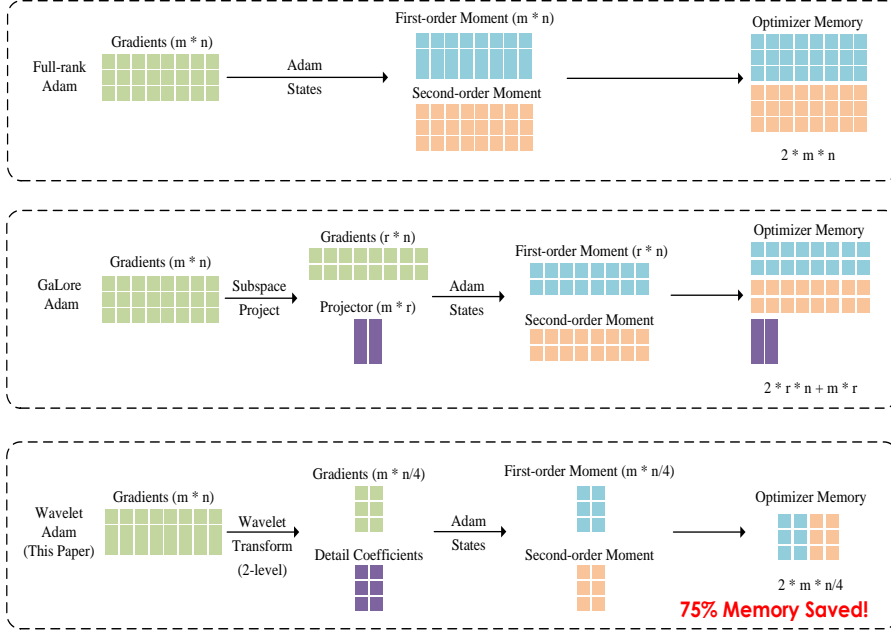


Fig. 1 Visualization of memory usage for Adam optimizer states. Compared with full-rank Adam, 2-level wavelet transform can reduce the optimizer state up to 75%. Moreover, wavelet requires no additional memory to retain an additional project matrix.

To address these challenges, Fira [14] introduces the error residual between the full-rank gradient and its subspace projection, while GoLore [18] enhances GaLore by utilizing random projection to better capture gradient information when noise is dominant. However, these methods still rely on SVD for updating the subspace, and the high computational cost of SVD ($O(m \times n^2)$ for a matrix of size $m \times n$) can significantly slow down training, particularly for large models. For example, updating a single subspace may take over ten minutes for the LLaMA 7B model, while inference typically only takes a few seconds [19]. To mitigate this issue, APOLLO [19] proposes an SVD-free variant of GaLore, replacing SVD with random projections. This modification improves both GaLore’s experimental performance and its training speed. Intuitively, the loss of information suggests that low-rank methods should perform worse in training compared to full-rank methods. Surprisingly, Fira and APOLLO outperformed full-rank training in extensive experiments, highlighting the potential of memory-efficient algorithms as alternatives to full-rank methods, which makes memory-efficient training meaningful.

The above methods are based on low-rank decomposition. Aside from low-rank decomposition, Wavelet Transform (WT) [20] also has wide applications in the field of compression. Compared with low-rank decomposition, wavelet transform has lower computational complexity ($O(m \times n)$), better captures local information features, and suppresses high-frequency noise [21]. Moreover, due to its robustness to noise, it is

better suited for stochastic gradient descent, a training model method that involves noise. Therefore, we can naturally raise the following question: *Can wavelet decomposition, like SVD decomposition, benefit the training of large language models, reducing memory consumption and improving model performance?*

In this paper, we explore memory-efficient training methods that extend beyond low-rank techniques. Inspired by the successful use of WT in image compression [22, 23], we introduce Gradient Wavelet Transform (GWT), a plug-and-play framework that applies wavelet transforms to gradients, effectively compressing the dimension and reducing the memory required for storing optimizer states. To illustrate the effectiveness of GWT, we provide a comparison with GaLore and full-rank Adam in terms of memory usage, as shown in Figure 1. Experimentally, we demonstrate that GWT performs well in both pre-training and fine-tuning tasks. Notably, when pre-training LLaMA models on the C4 dataset [24], GWT outperforms full-rank methods, achieving up to a 67% reduction in optimizer memory usage while accelerating training speed with our 2-level GWT on LLaMA 1B. Furthermore, we show that GWT is a versatile framework that can be integrated with optimizers beyond Adam, providing a general solution for memory-efficient training.

2 Results

In this section, we demonstrate that the GWT, as a memory-efficient optimization technique, can achieve performance on par with or even surpassing that of full-rank optimizers, while significantly reducing memory usage and increasing training throughput. Specifically, we evaluate GWT in two contexts: pre-training LLaMA [11] models on the Colossal Clean Crawled Corpus (C4) [24] English benchmark, and fine-tuning the RoBERTa-base model [25] on the General Language Understanding Evaluation (GLUE) [26] benchmark. Additionally, we present an ablation study to explore the impact of hyperparameters, including α , learning rate (lr), and the GWT level l .

For the GWT implementation, we employ the discrete Haar and discrete Daubechies-2 (DB2) wavelets as filters. A detailed description of the experimental setup can be found in Appendix A.

2.1 Pre-training LLaMA on C4

We integrate our Gradient Wavelet Transform (GWT) method with the Adam optimizer [10], using default hyperparameters ($\beta_1 = 0.9$, $\beta_2 = 0.999$, $\epsilon = 10^{-6}$), to evaluate its performance against existing memory-efficient algorithms on LLaMA models for the C4 pre-training task. For a comprehensive comparison, we include our reproduced results for full-rank Adam [10] and GaLore, and reference results from prior works such as LoRA [13], ReLoRA [17], Fira [14], and APOLLO [19].

In all experiments, we use a learning rate of 0.01 for both GWT and GaLore and apply cosine annealing for the learning rate schedule. For GaLore-r, we set the model rank to 1/4 and 1/8 model rank, denoted as GaLore-1/4 and GaLore-1/8, corresponding to the use of a 2/3-level GWT. We follow the initialization strategy from prior works [12] to initialize the network weights and enable GWT in both the

Table 1 Final validation complexity (lower is better) and estimated memory usage on pre-training LLaMA models on the C4 dataset. We use Haar-2 to denote the Adam optimizer with a 2-level Haar GWT. We can see that Haar-2 outperforms the baseline methods, achieving comparable or even lower validation perplexity, while simultaneously using less memory. Results marked with * refer to those values published in prior works.

Method	60M	130M	350M	1B
Full-Rank	33.37 (0.36G)	25.08 (0.76G)	18.75 (2.06G)	16.10 (7.80G)
Haar-2	29.35 (0.24G)	22.47 (0.52G)	16.29 (1.22G)	13.50 (4.38G)
DB2-2	29.60 (0.24G)	22.59 (0.52G)	16.30 (1.22G)	13.74 (4.38G)
GaLore-1/4	39.94 (0.24G)	26.47 (0.52G)	19.36 (1.22G)	15.66 (4.38G)
Haar-3	29.81 (0.22G)	22.63 (0.48G)	16.35 (1.08G)	- (3.81G)
DB2-3	30.01 (0.22G)	22.68 (0.48G)	17.98 (1.08G)	- (3.81G)
GaLore-1/8	48.48 (0.22G)	30.02 (0.48G)	21.59 (1.08G)	- (3.81G)
APOLLO* [19]	31.55 (0.24G)	22.84 (0.52G)	16.67 (1.22G)	14.10 (4.38G)
Fira* [14]	31.06 (0.24G)	22.73 (0.52G)	17.03 (1.22G)	14.31 (4.38G)
Low-Rank* [12]	78.18 (0.26G)	45.51 (0.54G)	37.41 (1.08G)	142.53 (3.57G)
LoRA* [12]	34.99 (0.36G)	33.92 (0.80G)	25.58 (1.76G)	19.21 (6.17G)
ReLoRA* [12]	37.04 (0.36G)	29.37 (0.80G)	29.08 (1.76G)	18.33 (6.17G)
Training Tokens	1.1B	2.2B	6.4B	13.1B

Multi-Layer Perceptron (MLP) and attention modules of the model. Haar and DB2 wavelets are used as basis functions, with Haar-2 specifically referring to the optimizer with a 2-level Haar transform.

The final validation perplexity and estimated memory usage for all methods are summarized in Table 1. Experimental results show that GWT consistently achieves lower validation perplexity while reducing memory usage compared to other memory-efficient baselines. In all the pre-training cases, GWT outperforms full-rank optimizers, and GaLore performs relatively closely to GWT. The choice of wavelet filter, whether Haar or DB2, does not have a significant impact on the final experimental results. Specifically, in the LLaMA 1B pre-training experiment, our 2-level GWT method reduces the total memory cost by 43.8% and the optimizer memory cost by 65.7% (from 7.80GB to 4.38GB on LLaMA 1B). Even with the use of 3-level GWT, our method still achieves experimental results that surpass full-rank, while reducing total memory consumption by up to 50%. In the same scenario, the gap between GaLore-1/8 and full-rank is further widened. Details of the memory estimation are presented in Appendix A.3.

In addition to the final evaluation metrics, we present learning curves for the pre-training task on LLaMA 60M-350M with varying memory costs in Figure 2. These curves show that GWT consistently outperforms both full-rank Adam and GaLore across different levels of wavelet transformation. In most cases, GaLore consistently shows a significant gap compared to full-rank Adam, while all GWT methods maintain

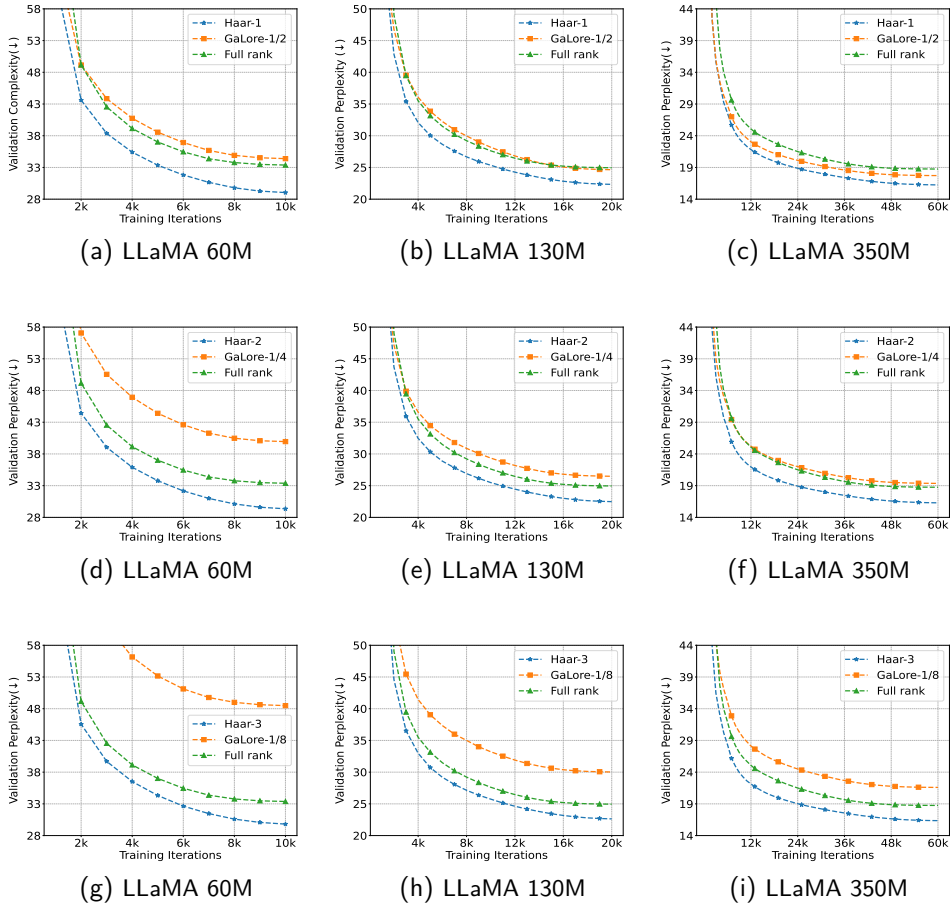


Fig. 2 Applying GWT to Adam optimizer for pre-training various LLaMA models with different memory usage. The results are presented as validation perplexity versus training iterations, with each memory-efficient algorithm evaluated within the same memory usage constraints. (a)-(c): Comparison of Haar-1 and GaLore-1/2. (d)-(f): Comparison of Haar-2 and GaLore-1/4. (g)-(i): Comparison of Haar-3 and GaLore-1/8.

results surpassing full-rank. Moreover, GWT not only achieves lower final validation perplexity but also accelerates convergence compared to the baselines.

We also extend our method to the Adafactor optimizer [27] and present the corresponding experimental results in Figure 6. These results demonstrate that, compared to GaLore, GWT achieves both lower validation perplexity and performance closer to that of the full-rank optimizer. This highlights the versatility and effectiveness of our method when integrated with other optimizers, showcasing its broad applicability in memory-efficient optimization.

Beyond final validation perplexity and memory usage, we also evaluate token throughput during the pre-training of the LLaMA 1B model using Haar-2, GaLore,

Table 2 Pre-training LLaMA 1B on C4. We report the validation perplexity on different iterations and the token throughput (per GPU).

	20K	40K	60K	80K	Tokens/s
Haar-2	18.34	15.76	14.47	13.72	2.825K
GaLore	20.37	17.82	16.44	15.79	2.518K
Full-Rank	21.77	18.19	16.71	16.16	1.259K
Tokens (B)	2.6	5.2	7.8	10.4	

and full-rank Adam. The experimental results are summarized in Table 2. Our method (Haar-2) achieves a training throughput of 2.825K tokens per second on GPU, providing more than a 2x speedup on throughput compared to full-rank Adam and approximately a 12% speedup relative to GaLore. This demonstrates that, in addition to its memory efficiency, the GWT method significantly accelerates training throughput, making it a highly efficient alternative to traditional optimization methods for large-scale pre-training tasks.

2.2 Fine-Tuning on GLUE Benchmarks

In this section, we further evaluate our method by fine-tuning the RoBERTa-base model on the GLUE benchmark. We report performance metrics across various tasks: accuracy for MNLI, Matthew’s correlation for CoLA, Pearson correlation for STS-B, F1 score for MRPC, and accuracy for the remaining tasks. It is important to note that the optimizer memory ratio during fine-tuning is typically very low, such as 1/96. For GWT, this would require approximately 7 wavelet transformations, which introduces significant computational overhead and contradicts the original intent of GWT. Therefore, for a fair comparison, we use GaLore-1/4 and Haar-2, referencing the results from LoRA and full-rank Adam as reported in prior work [12]. In the fine-tuning task, our primary focus is on evaluating the effectiveness of GWT. There is, however, considerable potential for accelerating multi-level GWT, which we plan to explore in future work.

The experimental results are presented in Table 3. As shown, GWT proves to be effective not only for pre-training but also for fine-tuning, offering competitive performance across multiple GLUE tasks. In contrast, LoRA is primarily designed for fine-tuning tasks and does not exhibit the same versatility across both pre-training and fine-tuning stages as GWT does.

2.3 Hyperparameter Study

In this section, we investigate the effects of the hyperparameters α and GWT level l . A more detailed discussion of these two hyperparameters is provided in Section 4.4.

Scale α . We evaluate Adam with 2-level Haar GWT using different values of α at a fixed learning rate ($lr = 0.01$). As shown in Figure 3a and 3b, we observe that our GWT is invariant to the hyperparameter. For α values larger than 0.1, the final experimental results remain relatively stable and do not differ significantly. Based

Table 3 Fine-tuning on GLUE benchmark using pre-trained RoBERTa-Base model. We present the final validation and average scores for all tasks (higher is better). * indicates results published in prior works.

	CoLA	STS-B	MRPC	RTE	SST2	MNLI	QNLI	QQP	Avg.
Full-Rank*	62.24	90.92	91.30	79.42	94.57	87.18	92.33	92.28	86.28
Haar-2	62.57	91.16	93.26	79.42	94.26	87.37	92.53	91.94	86.56
GaLore	61.32	91.13	92.41	77.25	94.03	86.77	92.56	91.77	85.90
LoRA* [12]	61.83	90.80	91.90	79.06	93.46	86.94	92.25	91.22	85.93

on the network initialization strategy we used, most modules in the network have a learning rate greater than 0.001 ($lr \times \alpha$). In contrast to Adam, which often requires a learning rate smaller than 0.001 to avoid loss spikes, GWT shows significantly better robustness to higher learning rates. For fine-tuning tasks, tuning α is equivalent to adjusting the learning rate (lr) hyperparameter based on our strategy. A detailed study of the learning rate hyperparameters (lr, α) on fine-tuning tasks is presented in Appendix A.2.

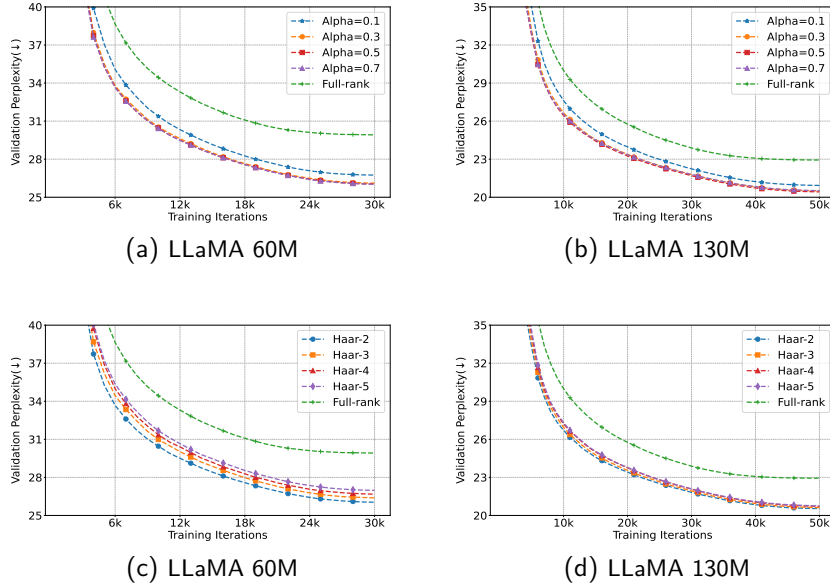


Fig. 3 Study the effects of α and l with Haar-2 on pre-training LLaMA 60M and 130M models.

GWT level l . We investigate the effects of the GWT level hyperparameter l , with the corresponding validation perplexity curves shown in Figure 3c and 3d. We found that the value of l has little impact on the final experimental results, and lower values

of l are only slightly better than others. One question that arises from the experimental results is whether the approximation coefficients are not crucial when using wavelets to compress gradients in LLM training, but rather the detail coefficients. The main impact of l seems to be on memory usage and throughput. The throughput results and optimizer memory estimate for different GWT levels are summarized in Table 4, demonstrating the trade-off between memory efficiency and model performance. Higher wavelet levels improve memory usage, but this may come at the cost of slightly higher validation perplexity and slower training speed.

Table 4 Estimated optimizer memory usage and token throughput (per GPU) with different GWT levels. Higher GWT levels lead to slower training token throughput but smaller memory usage.

Methods	60M		130M		350M	
	Memory	Tokens/s	Memory	Tokens/s	Memory	Tokens/s
Haar-1	0.16G	95.8K	0.36G	46.0K	0.81G	12.7K
Haar-2	0.12G	91.9K	0.28G	45.1K	0.54G	12.1K
Haar-3	0.10G	90.1K	0.24G	44.8K	0.40G	11.5K
Haar-4	0.09G	84.2K	0.22G	43.8K	0.33G	10.8K
Haar-5	0.08G	83.5K	0.21G	41.5K	0.29G	9.25K

3 Discussion

In this paper, we investigate memory-efficient optimization algorithms that extend beyond conventional low-rank decomposition and quantization techniques. Drawing inspiration from the limitations of current optimization methods and the proven success of WT in image and signal processing, we propose a unified framework that integrates GWT into standard optimizers. This framework bridges the gap between gradient compression and wavelet transforms, enabling more efficient training of LLMs by reducing memory usage and accelerating training speed.

To evaluate the effectiveness of our approach, we integrate GWT into the Adam [10] and Adafactor [27] optimizers. Our experimental results show that GWT achieves state-of-the-art performance across multiple stages of the LLM training process and is fully compatible with other optimizers beyond Adam. This gradient compression technique not only improves final validation scores but also enhances throughput, offering a novel memory-performance trade-off that complements existing methods, particularly those based on low-rank optimizations.

Our proposed GWT and its implementation draw inspiration from GaLore [12]. Both GWT and GaLore are closely related to Projected Gradient Descent (PGD) [28, 29], which projects the gradient onto a subspace before performing the update. However, there are key distinctions between GWT and GaLore. The primary difference lies in the projection operation: GWT not only projects the gradient onto the subspace but also leverages additional information from this projection, such as the

detail coefficients D_t (as shown in Eq. (6)). In contrast, GaLore discards the remaining information after projecting the gradient onto the subspace. When projecting back from the subspace to the gradient space, GWT retains more of the original gradient information. Importantly, this additional information is temporary and generated during the wavelet transform process itself, so it does not require extra storage. In summary, GWT provides an effective solution to the memory challenges encountered in training large models.

Here, we outline several intriguing open problems related to GWT: (a) The theoretical foundations behind GWT’s effectiveness in training remain unexplored. A deeper analysis of the method’s convergence and the limitations associated with its use is critical for refining its application and gaining a more comprehensive understanding of its behavior within optimization frameworks. (b) The wavelet transform operations themselves still require optimization. Wavelets were originally designed for time-series signals and images, raising the question: Can a specialized wavelet transform be developed to handle gradients, which are inherently more disordered and chaotic? Additionally, since the impact of l on the experimental results is minimal, the main effect of higher-order GWT lies in throughput, while offering higher memory efficiency. Therefore, the potential of GWT with higher l values is worth exploring. Given the linear properties of the Haar wavelet in GWT, is it possible to accelerate multi-level wavelet transforms to achieve even higher memory compression ratios, such as 1/64 or 1/128? (c) Finally, the applicability and effectiveness of GWT in other domains, such as vision models [30, 31] and diffusion models [32, 33], remain to be validated.

4 Methods

In this section, we first provide an overview of the basic theory behind the wavelet transform. We then explain how the GWT method is applied to the Adam optimizer [10], followed by a discussion of a unified framework that enables the integration of GWT into other optimizers, such as Adafactor [27]. We also cover the associated hyperparameters for GWT.

4.1 Discrete Haar Wavelet Transform

Wavelet transforms can be categorized into continuous and discrete types. In this paper, we focus on the 1-dimensional Discrete Haar wavelet Transform (DHT) as a case to illustrate our approach. DHT is one of the simplest and most widely used wavelet transforms in signal and image processing due to its low computational cost [34]. The DHT decomposes a signal (or image) into two components: a) Approximation coefficients (Low-frequency): Which represent the smooth or average part of the signal/image. b) Detail coefficients (High-frequency): Capture the difference or finer details of the signal/image.

For example, for an input signal or image represented by the sequence of values $[x_1, x_2, x_3, x_4, x_5, x_6, x_7, x_8]$, the 1-level DHT (Haar-1) computes the approximation

and detail coefficients as follows

$$\begin{aligned} \text{Approximation coefficient: } A_1 &= \left[\frac{x_1 + x_2}{2}, \frac{x_3 + x_4}{2}, \frac{x_5 + x_6}{2}, \frac{x_7 + x_8}{2} \right], \\ \text{Detail coefficient: } D_1 &= \left[\frac{x_1 - x_2}{2}, \frac{x_3 - x_4}{2}, \frac{x_5 - x_6}{2}, \frac{x_7 - x_8}{2} \right]. \end{aligned} \quad (1)$$

The wavelet filter for DHT are $[\frac{1}{2}, \frac{1}{2}]$ for approximation, and $[\frac{1}{2}, -\frac{1}{2}]$ for detail coefficients. The reconstruction of the original signal can be expressed as follows

$$[x_1, x_3, x_5, x_7] = A_1 + D_1, [x_2, x_4, x_6, x_8] = A_1 - D_1. \quad (2)$$

Next, we can apply an additional DHT transform to the approximation coefficient A_1 , yielding the following results:

$$\begin{aligned} A_2 &= \left[\frac{x_1 + x_2 + x_3 + x_4}{4}, \frac{x_5 + x_6 + x_7 + x_8}{4} \right], \\ D_2 &= \left[\frac{x_1 + x_2 - x_3 - x_4}{4}, \frac{x_5 + x_6 - x_7 - x_8}{4} \right]. \end{aligned}$$

Therefore, we have derived a simple implementation of 2-level DHT, the corresponding reconstruction is similar to 1-level. The DHT converts a vector with eight elements into two vectors (A_1, D_1) of 4 elements each or three vectors (A_2, D_2, D_1) . Storing just approximation coefficients will reduce our memory cost by 50% or 75%. This process can be repeated iteratively, breaking the signal into increasingly finer levels of approximation and detail, facilitating efficient compression and storage.

Building on the derivation above, we can represent the Discrete DHT as a matrix projection. For a more general formulation, let $W \in \mathbb{R}^{m \times n}$ be a matrix (we suppose $n \bmod 2 = 0$ for simplicity). The DHT and reconstruction can be expressed as:

$$[A, D] = WH, \quad W = [A, D]\tilde{H}, \quad (3)$$

where $A, D \in \mathbb{R}^{m \times \frac{n}{2}}$, $H, \tilde{H} \in \mathbb{R}^{n \times n}$ denote the Haar wavelet transform matrix, and the elements are defined as:

$$\begin{aligned} H_{2i-1, i} = H_{2i, i} = H_{2i-1, \frac{n}{2}+i} &= \frac{1}{2}, & H_{2i, \frac{n}{2}+i} &= -\frac{1}{2}, & 1 \leq i \leq \frac{n}{2}, \\ \tilde{H}_{i, i} = \tilde{H}_{\frac{n}{2}+i, 2i-1} &= 1, & \tilde{H}_{\frac{n}{2}+i, 2i} &= -1, & 1 \leq i \leq \frac{n}{2}. \end{aligned}$$

It is straightforward that $H\tilde{H} = I$, where I is the identity matrix. For higher-level DHT, the formulation is similar. This matrix-based representation allows for efficient computation and generalization of the DHT to higher-dimensional cases, making it a powerful tool for applications such as gradient compression in optimization methods.

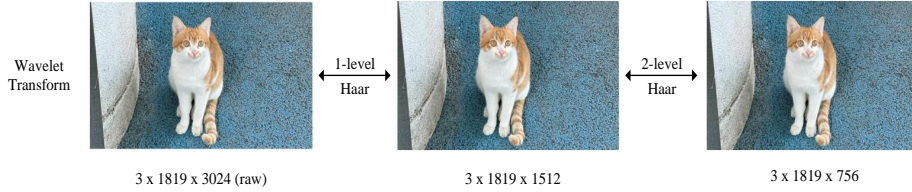


Fig. 4 Visualization of the approximation coefficients of a 2-Level DHT on an image (rescaled for visual clarity). Even after reducing the image to 25% of its original size (right), the approximation coefficients successfully preserve the key structural features of the image. This demonstrates the effectiveness of the DHT for applications such as image compression and other tasks requiring memory efficiency.

4.2 Adam with GWT

The Adam optimizer [10] adaptively adjusts the learning rates for each parameter based on its past gradient states, while also incorporating momentum to accelerate training. The update rule for the weights is given by the following recursive equation:

$$W_{t+1} = W_t - \eta \cdot \tilde{G}_t, \quad (4)$$

where $\eta > 0$ denotes the learning rate, \cdot represents the element-wise multiplication, $W \in \mathbb{R}^{m \times n}$ and

$$M_t = \beta_1 \cdot M_{t-1} + (1 - \beta_1) \cdot G_t, V_t = \beta_2 \cdot V_{t-1} + (1 - \beta_2) \cdot G_t^2, \tilde{G}_t = \frac{M_t}{\sqrt{V_t + \epsilon}}. \quad (5)$$

Here, $\beta_1, \beta_2 \in [0, 1)$ are the decay rates hyperparameters which are set as 0.9, 0.999 commonly, $\epsilon > 0$ to preserve numerical stability, $G_t \in \mathbb{R}^{m \times n}$ denotes the batch gradient at time step t , $G_t^2, M_t/\sqrt{V_t + \epsilon}$ represents the element-wise multiplication and division, and $M, V \in \mathbb{R}^{m \times n}$ represents the first/second-order moment in Adam optimizer.

For ease of presentation, we adopt a 1-level DHT in the following discussion. To integrate GWT with the Adam optimizer, we begin by applying GWT to the gradient matrix G_t at time step t (Eq. (3)), focusing on the approximate coefficients. This results in a compressed gradient matrix (approximation coefficient) $A_t \in \mathbb{R}^{m \times \frac{n}{2}}$ and a detail coefficient matrix $D_t \in \mathbb{R}^{m \times \frac{n}{2}}$. We then update the Adam states by replacing the original gradient G_t in the update rule (Eq. (5)) with the smaller matrix A_t to calculate \tilde{G}_t . To preserve the consistency of the state update, we scale the wavelet detail coefficients D_t by dividing them by D_t by $\sqrt{V_t + \epsilon}$ based on the linear properties of DHT (Eq. (3)). Finally, project \tilde{G}_t back to the original space and update the weights. The update rule can be rewritten by the following

$$[A_t, D_t] = G_t H, M_t = \beta_1 \cdot M_{t-1} + (1 - \beta_1) A_t, V_t = \beta_2 V_{t-1} + (1 - \beta_2) A_t^2, \quad (6)$$

$$\tilde{A}_t = \frac{M_t}{\sqrt{V_t + \epsilon}}, \tilde{D}_t = \frac{D_t}{\sqrt{V_t + \epsilon}}, \tilde{G}_t = [\tilde{A}_t, \tilde{D}_t] \tilde{H}, W_{t+1} = W_t - \eta \cdot \tilde{G}_t.$$

The procedure for applying GWT to the Adam optimizer is outlined in Algorithm 4.2. We implement the Adam optimizer with Haar-2 on the LLaMA 60M and 130M models, and present the learning curve in Figure 5. We observe that the learning curve (blue) demonstrates a heavy spike around the 600th iteration in LLaMA 60M, and a twice spike in LLaMA 130M. This phenomenon is likely due to unstable gradients during the early stages of training, as observed in previous studies [14, 35]. To address this issue, we adopt the Norm-growth Limiter (NL) technique introduced by Fira [14], which stabilizes gradient growth. NL controls the ratio of the current gradient norm to the previous gradient norm by rescaling the current gradient as follows

$$\text{if } \frac{\|\tilde{G}_t\|}{\|\tilde{G}_{t-1}\|} > \gamma \text{ then } \tilde{G}_t \leftarrow \frac{\tilde{G}_t}{\|\tilde{G}_t\|} \cdot \gamma \cdot \|\tilde{G}_{t-1}\|,$$

where γ is a threshold that limits the gradient norm growth, we adopt $\gamma = 1.01$ by default. This technique is more effective than gradient clipping and significantly reduces the impact of unstable gradients in the early training stages. After introducing NL, the learning curve (orange) for our Haar-2 implementation becomes smoother, resulting in a lower training loss (from 3.41 to 3.37 in LLaMA 60M).

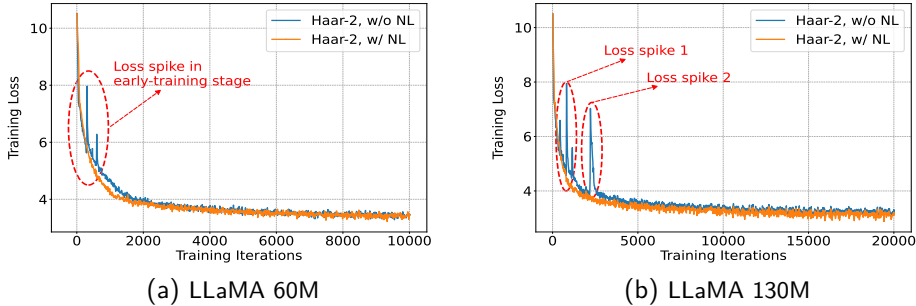


Fig. 5 Training loss comparison between Haar-2 with/without NL on LLaMA 60M and 130M.

In summary, we integrate the GWT method into the Adam optimizer, and it is theoretically observed that the memory occupied by the optimizer state can be reduced by up to 75%. GWT leverages a memory-efficient approach by projecting gradients into a subspace and performing optimizer state updates within that subspace. This reduces memory usage and can be applied to most optimizers that typically require significant memory for storing their states. Next, we will present a more general framework to incorporate the GWT method into a wider range of optimizers.

4.3 General Optimizer with GWT

In general, backpropagation in deep learning training follows the update rule:

Algorithm 1 Adam with Wavelet Transform

```
1: Input: Weight matrix  $W$ , step size  $\eta$ , batch size  $m$ , decay rates  $\beta_1, \beta_2$ , iteration
    $T$ ,  $\epsilon$  for numerical stability, scale factor  $\alpha$ , wavelet transform level  $l$ , and wavelet
   transformer  $H, \tilde{H}$ .
2: Initialize  $t \leftarrow 0$ 
3: repeat
4:    $G_t \leftarrow \frac{1}{m} \sum_{i=1}^m \nabla_W f_i(W_t)$  ▷ Batch gradient
5:    $[A_t, D_t] \leftarrow G_t H$  ▷ GWT for Approximation/Detail coefficients
6:   if  $t = 0$  then
7:     Initialize  $M_{-1} \leftarrow 0$  ▷ Initialize first-order moment
8:     Initialize  $V_{-1} \leftarrow 0$  ▷ Initialize second-order moment
9:   end if
10:  

---


11:  Adam states update
12:     $M_t \leftarrow \beta_1 \cdot M_{t-1} + (1 - \beta_1) \cdot A_t$  ▷ Update first-order moment
13:     $V_t \leftarrow \beta_2 \cdot V_{t-1} + (1 - \beta_2) \cdot A_t^2$  ▷ Update second-order moment
14:     $M_t \leftarrow M_t / (1 - \beta_1^t)$ 
15:     $V_t \leftarrow V_t / (1 - \beta_2^t)$  ▷ Bias correction
16:     $\tilde{A}_t \leftarrow M_t / (\sqrt{V_t} + \epsilon)$ 
17:     $\tilde{D}_t \leftarrow D_t / (\sqrt{V_t} + \epsilon)$  ▷ Coefficient correction
18:  

---


19:   $\tilde{G}_t \leftarrow \alpha \cdot [\tilde{A}_t, \tilde{D}_t] \tilde{H}$  ▷ Wavelet project back
20:   $W_t \leftarrow W_{t-1} + \eta \cdot \tilde{G}_t$  ▷ Update weights
21:   $t \leftarrow t + 1$ 
22: until  $t = T$ 
23: return  $W_t$ 
```

$$W_{t+1} = W_t - \eta \cdot \sum_{k=1}^t \tau_k(G_k), \quad (7)$$

where τ_k is a gradient regularizer dependent on optimizer states, which include state updates. Specifically, τ_k serves as an abstract representation of both first-order momentum and second-order momentum in Adam.

Building on the operation from the previous section, we first apply a GWT to the gradient G_k , yielding A_k and D_k (Eq. (3)). By substituting A_k into the optimizer state update and performing a reverse wavelet transform (multiply by \tilde{H}), we can naturally incorporate the GWT into the optimizer and the corresponding states. The update recursion with GWT can then be written as:

$$W_{t+1} = W_t - \eta \cdot \left[\sum_{k=1}^t \tau_k(A_k), D_t \right] \tilde{H}. \quad (8)$$

This equation captures the integration of wavelet transform-based adjustments into the optimizer's update rule. To this end, we have developed a unified update

Algorithm 2 Optimizer with GWT

- 1: **Input:** Weight matrix W , step size η , batch size m , regularizer τ_t , iteration T , transform level l , scale factor α , iteration T , wavelet transformer H, \tilde{H} .
 - 2: Initialize $t \leftarrow 0$
 - 3: **repeat**
 - 4: $G_t \leftarrow \frac{1}{m} \sum_{i=1}^m \nabla_W f_i(W_t)$
 - 5: $A_t, D_t \leftarrow G_t H$ ▷ GWT process
 - 6: $\tilde{A}_t \leftarrow \sum_{k=1}^t \tau_k(A_t)$ ▷ State update
 - 7: $\tilde{G}_t \leftarrow [\tilde{A}_t, D_t] \tilde{H}$ ▷ Reverse transform
 - 8: $W_t \leftarrow W_{t-1} + \eta \cdot \tilde{G}_t$
 - 9: **until** $t = T$
 - 10: **return** W_t
-

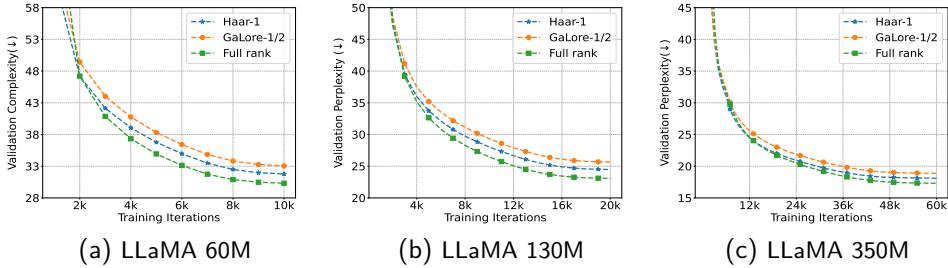


Fig. 6 Applying GWT to Adafactor optimizer for pre-training LLaMA 60M-350M models on C4. As observed, GWT can not only be applied on top of Adam but also achieve near full-rank performance on Adafactor.

schedule for optimizers with GWT based on linear formulation and demonstrated that GWT can be directly applied to existing optimizers with heavy-state memory usage. We present the unified framework for applying our GWT to optimizers in Algorithm 4.3. Therefore, we incorporate our GWT into Adafactor [27] optimizer for LLaMA pre-training tasks, and the experimental results are shown in Figure 6.

4.4 Additional Hyperparameters

In addition to the hyperparameters required by the original optimizer, several additional hyperparameters are needed to apply our GWT method. The hyperparameter α stands for the scale factor. Specifically, the scale hyperparameter α determines the magnitude of the update for the GWT module of $\eta \cdot \alpha$ (η for the modules without GWT). The H, \tilde{H} hyperparameters depend on the GWT basis used in the process (e.g., Haar, DB2, Rbio2.6, etc.). The choice of filter impacts the transformation applied during the wavelet decomposition and reconstruction. l stands for the GWT level, 1 denotes 1-level GWT which can reduce the optimizer memory up to 50%, and 2 denotes 2-level GWT which reduces the memory usage up to 75%, respectively.

These levels allow for varying degrees of memory reduction depending on the depth of the wavelet decomposition applied. Larger l can bring higher memory reduction but influence the throughput. These additional hyperparameters allow for more flexibility in applying GWT to different optimization problems while controlling the trade-off between memory usage and update precision.

References

- [1] Brown, T.B., Mann, B., Ryder, N., Subbiah, M., Kaplan, J., Dhariwal, P., Neelakantan, A., Shyam, P., Sastry, G., Askell, A., Agarwal, S., Herbert-Voss, A., Krueger, G., Henighan, T., Child, R., Ramesh, A., Ziegler, D.M., Wu, J., Winter, C., Hesse, C., Chen, M., Sigler, E., Litwin, M.-t., Gray, S., Chess, B., Clark, J., Berner, C., McCandlish, S., Radford, A., Sutskever, I., Amodei, D.: Language models are few-shot learners. ArXiv **abs/2005.14165** (2020)
- [2] Matthews, D., Spence, M., Mater, A., Nichols, J., Pulsford, S., Sandhu, M., Kaczmarewski, J., Miton, C., Tokuriki, N., Jackson, C.: Leveraging ancestral sequence reconstruction for protein representation learning. *Nature Machine Intelligence* **6**(12), 1542–1555 (2024)
- [3] Boiko, D.A., MacKnight, R., Kline, B., Gomes, G.: Autonomous chemical research with large language models. *Nature* **624**(7992), 570–578 (2023)
- [4] Méndez-Lucio, O., Nicolaou, C.A., Earnshaw, B.: Mole: a foundation model for molecular graphs using disentangled attention. *Nature Communications* **15**(1), 9431 (2024)
- [5] Ferber, D., Wölflein, G., Wiest, I.C., Ligerio, M., Sainath, S., Ghaffari Laleh, N., El Nahhas, O.S., Müller-Franzes, G., Jäger, D., Truhn, D., *et al.*: In-context learning enables multimodal large language models to classify cancer pathology images. *Nature Communications* **15**(1), 10104 (2024)
- [6] Qiu, P., Wu, C., Zhang, X., Lin, W., Wang, H., Zhang, Y., Wang, Y., Xie, W.: Towards building multilingual language model for medicine. *Nature Communications* **15**(1), 8384 (2024)
- [7] Mischler, G., Li, Y.A., Bickel, S., Mehta, A.D., Mesgarani, N.: Contextual feature extraction hierarchies converge in large language models and the brain. *Nature Machine Intelligence*, 1–11 (2024)
- [8] Wu, Z., Zhang, O., Wang, X., Fu, L., Zhao, H., Wang, J., Du, H., Jiang, D., Deng, Y., Cao, D., *et al.*: Leveraging language model for advanced multiproperty molecular optimization via prompt engineering. *Nature Machine Intelligence*, 1–11 (2024)
- [9] Hofmann, V., Kalluri, P.R., Jurafsky, D., King, S.: Ai generates covertly racist decisions about people based on their dialect. *Nature* **633**(8028), 147–154 (2024)

- [10] Kingma, D.P., Ba, J.: Adam: A method for stochastic optimization. CoRR **abs/1412.6980** (2014)
- [11] Touvron, H., Martin, L., Stone, K.R., Albert, P., Amjad Almahairi, e.a.: Llama 2: Open foundation and fine-tuned chat models. ArXiv **abs/2307.09288** (2023)
- [12] Zhao, J., Zhang, Z., Chen, B., Wang, Z., Anandkumar, A., Tian, Y.: Galore: Memory-efficient llm training by gradient low-rank projection. arXiv preprint arXiv:2403.03507 (2024)
- [13] Hu, E.J., Shen, Y., Wallis, P., Allen-Zhu, Z., Li, Y., Wang, S., Wang, L., Chen, W.: Lora: Low-rank adaptation of large language models. In: International Conference on Learning Representations (2022)
- [14] Chen, X., Feng, K., Li, C., Lai, X., Yue, X., Yuan, Y., Wang, G.: Fira: Can we achieve full-rank training of llms under low-rank constraint? ArXiv **abs/2410.01623** (2024)
- [15] Zhang, L., Zhang, L., Shi, S., Chu, X., Li, B.: Lora-fa: Memory-efficient low-rank adaptation for large language models fine-tuning. arXiv preprint arXiv:2308.03303 (2023)
- [16] Xia, W., Qin, C., Hazan, E.: Chain of lora: Efficient fine-tuning of language models via residual learning. arXiv preprint arXiv:2401.04151 (2024)
- [17] Lialin, V., Shivagunde, N., Muckatira, S., Rumshisky, A.: Relora: High-rank training through low-rank updates. In: International Conference on Learning Representations (2023)
- [18] He, Y., Li, P., Hu, Y., Chen, C., Yuan, K.: Subspace optimization for large language models with convergence guarantees. arXiv preprint arXiv:2410.11289 (2024)
- [19] Zhu, H., Zhang, Z., Cong, W., Liu, X., Park, S., Chandra, V., Long, B., Pan, D.Z., Wang, Z., Lee, J.: APOLLO: SGD-like Memory, AdamW-level Performance (2024)
- [20] Burrus, C.S., Gopinath, R.A., Guo, H.: Wavelets and wavelet transforms. rice university, houston edition **98** (1998)
- [21] Rioul, O., Vetterli, M.: Wavelets and signal processing. IEEE Signal Processing Magazine **8**(4), 14–38 (1991) <https://doi.org/10.1109/79.91217>
- [22] Deever, A.T., Hemami, S.S.: Lossless image compression with projection-based and adaptive reversible integer wavelet transforms. IEEE transactions on image processing **12**(5), 489–499 (2003)
- [23] Razavikia, S., Amini, A., Daei, S.: Reconstruction of binary shapes from blurred

- images via hankel-structured low-rank matrix recovery. *IEEE Transactions on Image Processing* **29**, 2452–2462 (2019)
- [24] Raffel, C., Shazeer, N.M., Roberts, A., Lee, K., Narang, S., Matena, M., Zhou, Y., Li, W., Liu, P.J.: Exploring the limits of transfer learning with a unified text-to-text transformer. *J. Mach. Learn. Res.* **21**, 140–114067 (2019)
- [25] Liu, Y.: Roberta: A robustly optimized bert pretraining approach. arXiv preprint arXiv:1907.11692 **364** (2019)
- [26] Wang, A., Singh, A., Michael, J., Hill, F., Levy, O., Bowman, S.R.: Glue: A multi-task benchmark and analysis platform for natural language understanding. In: *BlackboxNLP@EMNLP* (2018)
- [27] Shazeer, N.M., Stern, M.: Adafactor: Adaptive learning rates with sublinear memory cost. *ArXiv abs/1804.04235* (2018)
- [28] Chen, Y., Wainwright, M.J.: Fast low-rank estimation by projected gradient descent: General statistical and algorithmic guarantees. *ArXiv abs/1509.03025* (2015)
- [29] Chen, H., Raskutti, G., Yuan, M.: Non-convex projected gradient descent for generalized low-rank tensor regression. *J. Mach. Learn. Res.* **20**, 5–1537 (2016)
- [30] Dosovitskiy, A., Beyer, L., Kolesnikov, A., Weissenborn, D., Zhai, X., Unterthiner, T., Dehghani, M., Minderer, M., Heigold, G., Gelly, S., Uszkoreit, J., Houlsby, N.: An image is worth 16x16 words: Transformers for image recognition at scale. *ICLR* (2021)
- [31] Liu, Z., Lin, Y., Cao, Y., Hu, H., Wei, Y., Zhang, Z., Lin, S., Guo, B.: Swin transformer: Hierarchical vision transformer using shifted windows. In: *Proceedings of the IEEE/CVF International Conference on Computer Vision*, pp. 10012–10022 (2021)
- [32] Ho, J., Jain, A., Abbeel, P.: Denoising diffusion probabilistic models. *Advances in neural information processing systems* **33**, 6840–6851 (2020)
- [33] Song, Y., Sohl-Dickstein, J., Kingma, D.P., Kumar, A., Ermon, S., Poole, B.: Score-based generative modeling through stochastic differential equations. In: *International Conference on Learning Representations* (2021)
- [34] Porwik, P., Lisowska, A.: The haar-wavelet transform in digital image processing: Its status and achievements. *Machine graphics & vision* **13**, 79–98 (2004)
- [35] Molybog, I., Albert, P., Chen, M., DeVito, Z., Esiobu, D., Goyal, N., Koura, P.S., Narang, S., Poulton, A., Silva, R., Tang, B., Liskovich, D., Xu, P., Zhang, Y., Kambadur, M.H.M., Roller, S., Zhang, S.: A theory on adam instability in

- large-scale machine learning. ArXiv [abs/2304.09871](#) (2023)
- [36] Touvron, H., Lavril, T., Izacard, G., Martinet, X., Lachaux, M.-A., Lacroix, T., Rozière, B., Goyal, N., Hambro, E., Azhar, F., Rodriguez, A., Joulin, A., Grave, E., Lample, G.: Llama: Open and efficient foundation language models. ArXiv [abs/2302.13971](#) (2023)
 - [37] Vaswani, A., Shazeer, N.M., Parmar, N., Uszkoreit, J., Jones, L., Gomez, A.N., Kaiser, L., Polosukhin, I.: Attention is all you need. In: Neural Information Processing Systems (2017)
 - [38] Paszke, A., Gross, S., Chintala, S., Chanan, G., Yang, E., DeVito, Z., Lin, Z., Desmaison, A., Antiga, L., Lerer, A.: Automatic differentiation in pytorch (2017)
 - [39] Wolter, M., Blanke, F., Garcke, J., Hoyt, C.T.: ptwt - the pytorch wavelet toolbox. *Journal of Machine Learning Research* **25**(80), 1–7 (2024)
 - [40] Warstadt, A., Singh, A., Bowman, S.R.: Neural network acceptability judgments. *Transactions of the Association for Computational Linguistics* **7**, 625–641 (2018)
 - [41] Cer, D.M., Diab, M.T., Agirre, E., Lopez-Gazpio, I., Specia, L.: Semeval-2017 task 1: Semantic textual similarity multilingual and crosslingual focused evaluation. In: International Workshop on Semantic Evaluation (2017)
 - [42] Dolan, W.B., Brockett, C.: Automatically constructing a corpus of sentential paraphrases. In: International Joint Conference on Natural Language Processing (2005)
 - [43] Socher, R., Perelygin, A., Wu, J., Chuang, J., Manning, C.D., Ng, A., Potts, C.: Recursive deep models for semantic compositionality over a sentiment treebank. In: Conference on Empirical Methods in Natural Language Processing (2013)
 - [44] Williams, A., Nangia, N., Bowman, S.R.: A broad-coverage challenge corpus for sentence understanding through inference. In: North American Chapter of the Association for Computational Linguistics (2017)
 - [45] Rajpurkar, P., Jia, R., Liang, P.: Know what you don’t know: Unanswerable questions for squad. ArXiv [abs/1806.03822](#) (2018)

Appendix A Experiment Details

A.1 Network Architecture

In this section, we describe the network architectures of the LLaMA (Large Language Model Meta AI) [36] and RoBERTa (Robustly Optimized BERT Approach) [25] models, which complement the experimental details provided in the main text. LLaMA is a family of foundational language models based on transformers [37]. For this paper, we

adopt the LLaMA models from previous work [17], which use RMSNorm and SwiGLU activations [11, 36]. RoBERTa, on the other hand, is a variant of BERT (Bidirectional Encoder Representations from Transformers) [25], also built on the transformer architecture. Table A1 presents the architectural hyperparameters for the LLaMA and RoBERTa-base models, as well as the pre-training token amounts for LLaMA models across different sizes.

Table A1 Architecture hyperparameters of LLaMA and RoBERTa-base models pre-trained in this paper. Batch size and training data amount are specified in tokens.

Model	Params	Hidden	Intermediate	Heads	Layers	Iteration	Tokens
LLaMA	60M	512	1376	8	8	10K	1.3B
	130M	768	2048	12	12	20K	2.6B
	350M	1024	2736	16	24	60K	7.8B
	1B	2048	5461	24	32	100K	13.1B
RoBERTa	125M	768	3072	12	12	-	-

A.2 Experiment Hyperparameters

In this section, we provide detailed information on the hyperparameters and experimental setup used in the experiments discussed in the main text. For the LLaMA pre-training tasks, we follow the experimental configuration used in previous work [12], which employs the default Adam hyperparameters ($\beta_1 = 0.9, \beta_2 = 0.999, \epsilon = 10^{-6}$), a maximum sequence length of 256 tokens, and gradient accumulation with a batch size of 512. Additionally, we apply a learning rate warm-up for the first 10% of the iterations and use a cosine annealing schedule with the initial learning rate.

For the GWT method, we perform hyperparameter tuning on the scale parameter α from the set [0.1, 0.15, 0.2, 0.25], selecting the value that yields the best performance across all LLaMA pre-training tasks. We found that our method is not sensitive to scale, and setting α to 0.25 yields good results in most pretraining tasks, which is consistent with the hyperparameters used in previous work [12, 19]. For the baseline methods, we use their default hyperparameters: $\alpha = 0.25$ and $lr = 0.01$ for GaLore, and $lr = 0.001$ for Adam (0.0005 for Adam in LLaMA 1b). Consistent with prior work [12], we enable GWT and GaLore in the attention and MLP modules.

Finally, we summarize the hyperparameter α , the GPUs used (RTX 3090), and the training time (in hours) for our method required to reproduce the results shown of Table 1 in Table A2.

For the GLUE fine-tuning tasks, we set the α hyperparameter to 2 for both GWT and GaLore (enable GWT and GaLore in all modules). The lr for GWT is chosen from the interval $[1 \times 10^{-6}, 1 \times 10^{-5}]$, GaLore is tuned within the interval $[5 \times 10^{-6}, 5 \times 10^{-5}]$. For each GLUE task, we use a batch size of 16 (except for CoLA, where the batch size is 32), train for 30 epochs, and set the maximum sequence length to 512. We enable GWT and GaLore across all network modules for all tasks. We present the

Table A2 Hyperparameter α , training GPUs, and training time (hours) for different LLaMA models. We report the training time for Adam with our GWT, both GWT and GaLore adopt an initialization lr of 0.01.

	60M	130M	350M	1B
Haar-2	0.25	0.25	0.25	0.25
Haar-3	0.25	0.25	0.25	-
DB2-2	0.25	0.25	0.25	0.25
DB2-3	0.25	0.25	0.25	-
GaLore	0.25	0.25	0.25	0.25
GPUs (3090)	4	4	16	32
Time	0.99h	4.03h	11.83	40.18h

experimental results of our tuning process in Table A3 as an ablation study. The specific hyperparameters used for the GLUE fine-tuning tasks are summarized in the same Table. All experiments were conducted using a PyTorch [38] random seed of 1234 to ensure reproducibility.

For a fair comparison, we implement GaLore and GWT with an estimated 1/4 optimizer state memory usage. In prior work [12], GaLore was implemented with a rank of 4 and 8, which corresponds to less than 1/4 of the model rank. To achieve the same memory usage with GWT as in GaLore with rank 8, we found that GWT requires approximately a 7-level wavelet transform. Achieving ultra-low memory requirements with GWT, especially beyond the 1/4 model rank, will be explored in future work.

Table A3 GLUE benchmarks scores with different learning rates for Haar-2 and GaLore. We present the used learning rate for the results in Table 3.

Haar-2	CoLA	STS-B	MRPC	RTE	SST2	MNLI	QNLI	QQP
1E-06	57.01	90.19	90.55	76.17	94.03	86.95	92.45	91.46
2E-06	58.29	90.70	91.87	78.70	-	-	-	-
3E-06	59.81	91.07	92.09	79.42	93.92	87.07	92.51	91.84
4E-06	62.07	90.94	91.16	78.33	-	-	-	-
5E-06	62.57	91.16	93.18	75.81	94.26	87.37	92.53	91.81
6E-06	62.07	90.97	92.76	78.70	-	-	-	-
7E-06	59.43	90.70	92.36	73.64	94.15	97.35	92.38	91.94
8E-06	59.81	90.93	91.73	77.25	-	-	-	-
9E-06	59.30	90.84	93.26	77.25	92.31	86.84	92.30	91.78
1E-05	59.57	90.75	91.79	78.70	-	-	-	-
<i>lr</i>	5E-06	5E-06	7E-06	3E-06	5E-06	5E-06	5E-06	7E-06
Batch size	32	16	16	16	16	16	16	16

A.3 Experiment Environments

We adopt the BF-16 format for all the pre-training processes to reduce memory usage. All experiments were conducted on 1 to 8 server nodes, each equipped with four NVIDIA 3090 GPUs and Intel(R) Xeon(R) Gold 6226R CPU @ 2.90GHz. The Python version of 3.10, and the PyTorch [38] version of 2.3.0. We use the Pytorch toolbox for our GWT implementation [39].

A.4 Memory and Throughput Estimates

In this section, we provide an additional explanation of the GPU memory usage results reported in the paper. In practical computations, GPU memory usage is influenced by various factors, such as model size, batch size, optimizer states, PyTorch’s memory fragmentation management strategy, and model training strategies (single-GPU or multi-GPU), among others. Here, we estimate the GPU memory usage for the model weights and Adam optimizer states using bfloat16. Specifically, the memory usage for the weights of LLaMA 60M is 0.12G, while the optimizer occupies 0.23G of GPU memory. Since our GWT method primarily targets optimizing the memory usage of the optimizer, the weight memory usage for LLaMA 60M under the Adam optimizer with GWT remains 0.12G. From the perspective of optimizer states, the memory usage of the 2-level GWT should be equal to that of GaLore, which uses only 1/4 of the hidden size as the rank. In our experiments, we applied GWT or GaLore only to the attention and MLP modules of LLaMA. Therefore, the memory usage of the optimizer state also depends on the number of parameters in these two modules. We present the theoretical memory estimate of weight parameters and optimizer states for different methods and models in Table A4.

Besides the memory estimate, we also report the training throughput as a complement to the training speed report. For example, we pre-train LLaMA 60M with a total batch size of 512 and a max sequence length of 256 in 10,000 iterations. This is equivalent to a total token size of $512 \times 256 = 131072 \approx 131\text{K}$ and a total of $131072 \times 10000 = 1310720000 \approx 1.3\text{B}$ tokens during the whole training process. In Tables 4 and A2, we provide the training time and the number of GPUs used. Training LLaMA60M with our Haar-2 on four GPUs takes approximately 0.99 hours. Hence, we can compute the token throughput per GPU per second as $1310720000 / (0.99 \times 3600 \times 4) \approx 91.9\text{Ktokens/s}$

Appendix B Benchmark Details

In this section, we provide a detailed description of the benchmarks used in the paper, serving as a supplement to the results section 2.

C4 benchmark. We adopt Colossal Clean Crawled Corpus (C4) [24] benchmark of the English version for all the pre-training tasks. The C4 English benchmark is a colossal, cleaned version of Common Crawl’s web crawl corpus based on the Common Crawl dataset. Includes 305GB of English-language text and is mainly intended to pre-train language models. The validation complexity is obtained by taking the validation loss and exponentiating it with the base of Euler’s number e .

Table A4 Memory estimate of weight parameters/optimizer states. * indicates results published in prior works.

Method	60M	130M	350M	1B
Full-Rank*	0.12G/0.23G	0.25G/0.51G	0.68G/1.37G	2.60G/5.20G
GWT-2	0.12G/0.12G	0.25G/0.28G	0.68G/0.54G	2.60G/1.78G
GaLore	0.12G/0.12G	0.25G/0.28G	0.68G/0.54G	2.60G/1.78G
Low-Rank*	0.08G/0.17G	0.18G/0.37G	0.36G/0.72G	1.19G/2.38G
LoRA*	0.20G/0.17G	0.44G/0.37G	1.04G/0.72G	3.79G/2.38G
ReLoRA*	0.20G/0.17G	0.44G/0.37G	1.04G/0.72G	3.79G/2.38G

GLUE benchmark. We fine-tune RoBERTa-base model [25] on General Language Understanding Evaluation (GLUE) [26] benchmark. GLUE is a collection of resources for training, evaluating, and analyzing natural language understanding systems, including CoLA (The Corpus of Linguistic Acceptability, binary classification) [40], STS-B (Semantic Textual Similarity Benchmark, textual similarity regression) [41], MRPC (Microsoft Research Paraphrase Corpus, paraphrase detection) [42], RTE (Recognizing Textual Entailment, inference task), SST2 (Stanford Sentiment Treebank, sentiment analysis) [43], MNLI (Multi-Genre Natural Language Inference Corpus, textual entailment task) [44], QNLI (Stanford Question Answering Dataset, inference task) [45], QQP (question answering). The broad coverage makes GLUE a standard benchmark for evaluating pre-training BERT models [13].

Appendix C Availability

All models and benchmarks used in this paper are publicly available. The LLaMA models [11], a series of open-source large-scale models developed by Meta, can be accessed and downloaded from <https://www.llama.com/>. The network architecture details for these models are provided in Table A1, enabling independent initialization and training. For the fine-tuning task, we use the RoBERTa-base model [25], released by Facebook AI, which can be downloaded from HuggingFace at <https://huggingface.co/FacebookAI/roberta-base>. The C4 [24] dataset, used for the pre-training tasks, can be downloaded from <https://huggingface.co/datasets/allenai/c4> using the Datasets module or via git clone. The GLUE [26] benchmark can be accessed at <https://github.com/nyu-mll/GLUE-baselines> or through the tools provided by HuggingFace. Finally, the source code to reproduce our results is available at <https://github.com/zqOuO/GWT>.